Available online at www.sciencedirect.com
SCIENCE DIRECT®
International Journal of Solids and Structures 42 (2005) 4833–4858
INTERNATIONAL JOURNAL OF SOLIDS and STRUCTURES
www.elsevier.com/locate/ijsolstr

Algebraic tensegrity form-finding

Milenko Masic [a,*], Robert E. Skelton [a], Philip E. Gill [b,1]

[a] Department of Mechanical and Aerospace Engineering, University of California San Diego, La Jolla, CA 92093-0411, United States
[b] Department of Mathematics, University of California San Diego, La Jolla, CA 92093-0112, United States

Received 7 November 2003; received in revised form 18 January 2005
Available online 5 March 2005

Abstract

This paper concerns the form-finding problem for general and symmetric tensegrity structures with shape constraints. A number of different geometries are treated and several fundamental properties of tensegrity structures are identified that simplify the form-finding problem. The concept of a tensegrity invariance (similarity) transformation is defined and it is shown that tensegrity equilibrium is preserved under affine node position transformations. This result provides the basis for a new tensegrity form-finding tool. The generality of the problem formulation makes it suitable for the automated generation of the equations and their derivatives. State-of-the-art numerical algorithms are applied to solve several example problems. Examples are given for tensegrity plates, shell-class symmetric tensegrity structures and structures generated by applying similarity transformation.

Keywords: Tensegrity; Shape constraints; Symmetry; Nonlinear zero-finding

1. Introduction

A tensegrity structure is a prestressable truss-like system that, unlike regular trusses, involves both string and bar elements, connected with ball joints. The fundamental problems in designing a tensegrity structure are finding an equilibrium, and establishing the stability of the prestressed configuration.

Historically, tensegrity *form-finding* accounts for the major portion of the tensegrity research. Tibert and Pellegrino (2003) published an overview of available form-finding techniques. They compared different methods, established equivalency among them and discussed some potential shortcomings. They concluded

* Corresponding author. Tel.: +1 858 822 6679; fax: +1 858 822 3107.
E-mail address: mmasic@mae.ucsd.edu (M. Masic).
[1] The work of this author was partially supported by NSF grant CCF0082100.

0020-7683/$ - see front matter © 2005 Elsevier Ltd. All rights reserved.
doi:10.1016/j.ijsolstr.2005.01.014

Nomenclature

n_n, n_e	number of nodes and number of elements
$\mathbb{R}^n_m$	set of column vectors composed of n $m \times 1$ vectors
$\mathbb{N}$, $\mathbb{P}$, $\mathbb{E}$	sets of nodes, nodal vectors and elements
$\mathbf{p}_i \in \mathbb{R}^3$, $\mathbf{p} \in \mathbb{R}^{n_n}_3$	nodal vector and vector of nodal vectors
$\mathbf{g}_i \in \mathbb{R}^3$, $\mathbf{g} \in \mathbb{R}^{n_e}_3$	element vector and vector of element vectors
$C = [c_{ij}]^{n_e}_{n_n}$	reduced connectivity (node–element incidence) matrix
$M = [m_{ji}]^{n_n}_{n_e}$	member-node incidence matrix
$\mathbf{C} = C \otimes I_3$	connectivity (element force to nodal force mapping) matrix
$\mathbf{M} = M \otimes I_3$	matrix of nodal vector to element vector mapping
$\lambda_i \in \mathbb{R}$, $\boldsymbol{\lambda} \in \mathbb{R}^{n_e}$	force-density and force-density vector
$\underline{\mathbf{p}} \in \mathbb{R}^{n_{ne}}_3$	reduced nodal vector of symmetric structure
$\mathscr{R}$	mapping from reduced to full nodal vector
$\underline{\boldsymbol{\lambda}} \in \mathbb{R}^{n_{ee}}$	reduced force density vector of symmetric structure
$Q = [q_{ij}]^{n_{ee}}_{n_e}$	mapping from reduced to full force density vector
$\mathbf{D} = [d_{ij}]^{n_n}_{n_{ne}} \otimes I_3$	mapping from full to reduced set of equilibrium equations
$\tilde{\cdot}$	diagonalization operator
$z_i \in \mathbb{R}$, $\mathbf{z} \in \mathbb{R}^{n_e}$	element type identifier and vector of the identifiers
$l_i \in \mathbb{R}$, $\mathbf{l} \in \mathbb{R}^{n_e}$	element length and vectors of the lengths
$l_{0_i} \in \mathbb{R}$, $\mathbf{l}_0 \in \mathbb{R}^{n_e}$	element rest-length and vector of the rest-lengths
$y_i \in \mathbb{R}$, $\mathbf{y} \in \mathbb{R}^{n_e}$	element Young's modulus and vector of the moduli
$a_i \in \mathbb{R}$, $\mathbf{a} \in \mathbb{R}^{n_e}$	element cross-sectional area and vector of the areas
$(\cdot)_b$, $(\cdot)_s$	partitions of vectors corresponding to bars and strings
R	orthogonal matrix
n	number of bars in tower stage
r, $\mathbf{r}$	radius of tower stage and vector of the radii
t, $\mathbf{t}$	truncation ratio of tower stage and vector of the truncations
α, $\boldsymbol{\alpha}$	twist angle of tower stage and vector of the angles
β, $\boldsymbol{\beta}$	twist angle between tower stages and vector of the angles
γ, $\boldsymbol{\gamma}$	overlap between tower stages and vector of the overlaps
$\mathbf{n}$	vector perpendicular to plate plane
h	structure height
I	identity matrix
$\mathscr{I}(\cdot)$	isometric mapping

that all kinematic methods, including the dynamic relaxation proposed by Motro (1984), are restricted to less regular structures, that is, to structures with tensegrity geometry but with undesirable shape. They also suggested that the force-density method affords no control over the lengths of the elements of the structure.

Failure to explicitly include shape constraints in the form-finding problem is a deficiency of the force-density method in its present form. This method was adapted for tensegrity form-finding by Vasart and Motro (1999) from a similar method for the analysis of prestressed networks proposed by Schek (1974). In this form, the method concerns only shape constraints for the nodes that are attached to supports. The treatment of these constraints is essentially different from the general shape constraints that define the desired geometry of the equilibrium structure in the absence of constraint forces. While the boundary conditions allow for a reduction of the number of equilibrium equations (by introducing additional

variables as Lagrange multipliers in the problem), the general geometry constraints formulated as algebraic constraints must be enforced together with the full set of the equilibrium equations. For more details on the treatment of boundary conditions see Masic and Skelton (2004).

This paper extends the force-density method by explicitly including shape constraints in the problem and treating them jointly with the equilibrium conditions. Different symmetries of tensegrity structures are considered, together with their role in simplifying the formulation of form-finding problems. Connelly and Back (1998) and Connelly and Terrell (1995) studied the rigidity of several highly symmetric tensegrity representations of abstract symmetry groups, and Back and Connelly (1998) published their full catalog. In contrast to these results, our analysis focuses on identifying properties of general symmetric form-finding problems within the force-density framework with the aim of finding efficient large-scale solutions. In particular, necessary and sufficient conditions leading to the simplification of the problem are formulated. For example, our study shows that a symmetric structure may admit an asymmetric distribution of prestress as well as a symmetric prestress. This shows that the result of Hinrichs (1984), cited by Connelly and Terrell (1995)—that the symmetric tensegrity prisms with the least number of strings admit only symmetric prestress—is not a general result.

The second contribution of this paper is a theorem that shows that the tensegrity equilibrium is invariant under an affine transformation of nodal coordinates. This result allows the trivial equilibrium analysis of all tensegrities with the geometry defined using an affine transformation of a structure with known equilibrium geometry.

The outline of the paper is as follows. First, in Section 2, we define a compact formulation of the force-density method for tensegrity form-finding. Section 3 considers shape and symmetry constraints. In this section, several properties of symmetric tensegrity structures are analyzed and implemented in order to reduce the size and complexity of the problem. Section 4 introduces a class of geometric transformations that preserve equilibrium. A compact form of the stiffness matrix of a tensegrity structure is derived in Section 5. Section 6 offers several form-finding examples and our conclusions are discussed in Section 7.

2. The force-density method for tensegrity form-finding

The force-density formulation of the tensegrity equilibrium conditions presented in this section is essentially identical to that derived by Vasart and Motro (1999). These introductory considerations define some useful ideas and introduce vector operators used in later sections.

2.1. The geometry of a tensegrity structure

Definition 1. The *nodes* v_k, $k = 1,\ldots,n_n$, of a tensegrity structure are the points where bars and strings of the structure connect. A nodal vector $\mathbf{p}_k \in \mathbb{R}^3$ represents the position of the node v_k. The set of all nodes of a tensegrity structure and the associated set of nodal vectors are denoted by $\mathbb{N}$ and $\mathbb{P}$ respectively.

Definition 2. An *element* $e_i = \{[v_k, v_j], z_i\}$, $k \neq j$, $i = 1,\ldots,n_e$, of a tensegrity structure is either a bar or string that connects the two nodes v_k and v_j. The pair $[v_k, v_j]$ is an ordered pair, and z_i identifies the element type. For a tensegrity structure with the element set $\mathbb{E}$, z_i is defined such that

$$z_i = \begin{cases} 1, & \text{if } e_i \in \mathbb{E}_s, \\ -1, & \text{if } e_i \in \mathbb{E}_b, \end{cases} \tag{1}$$

where $\mathbb{E}_s \in \mathbb{E}$ and $\mathbb{E}_b \in \mathbb{E}$ are the sets of string and bar elements.

Definition 3. An *element vector* $\mathbf{g}_i \in \mathbb{R}^3$ is a vector along the length of an element $e_i = \{[v_k, v_j], z_i\}$. It emanates from the first node v_k and ends at the second node v_j of the element, i.e.,

$$\mathbf{g}_i = \mathbf{p}_j - \mathbf{p}_k.$$

It is obvious that the magnitude of an element vector $\mathbf{g}_i$ is equal to its length $\|\mathbf{g}_i\|$, denoted by l_i.

Let $\mathbb{R}^n_m$ denote the vector space of vectors $\mathbf{x}$ that have the following structure:

$$\mathbf{x} \in \mathbb{R}^n_m \;\Rightarrow\; \mathbf{x}^{\mathrm{T}} = \begin{bmatrix} \mathbf{x}_1^{\mathrm{T}} & \mathbf{x}_2^{\mathrm{T}} & \cdots & \mathbf{x}_n^{\mathrm{T}} \end{bmatrix}, \quad \mathbf{x}_i \in \mathbb{R}^m, \text{ with } \mathbb{R}^m = \mathbb{R}^m_1.$$

The vector $\mathbf{p} \in \mathbb{R}^{n_n}_3$ of nodal vectors is formed by collecting all node vectors $\mathbf{p}_i$, with similar definitions give the vector $\mathbf{g}(\mathbb{E}, \mathbb{P}) \in \mathbb{R}^{n_e}_3$ of element vectors and the vector $\mathbf{z} \in \mathbb{R}^{n_e}$ of individual element-type identifiers. It follows that

$$\mathbf{p}^{\mathrm{T}} = \begin{bmatrix} \mathbf{p}_1^{\mathrm{T}} & \mathbf{p}_2^{\mathrm{T}} & \cdots & \mathbf{p}_{n_n}^{\mathrm{T}} \end{bmatrix}, \quad \mathbf{g}^{\mathrm{T}} = \begin{bmatrix} \mathbf{g}_1^{\mathrm{T}} & \mathbf{g}_2^{\mathrm{T}} & \cdots & \mathbf{g}_{n_e}^{\mathrm{T}} \end{bmatrix}, \quad \text{and} \quad \mathbf{z}^{\mathrm{T}} = \begin{bmatrix} z_1 & z_2 & \cdots & z_{n_e} \end{bmatrix}.$$

2.1.1. The mapping from nodal position to element vector

We define the matrix $M(\mathbb{E}) \in \mathbb{R}^{n_e \times n_n}$ with elements m_{ij} as follows:

$$m_{ij} = \begin{cases} -1, & \text{if } v_j \text{ is the first node of the element } e_i, \\ 1, & \text{if } v_j \text{ is the second node of the element } e_i, \\ 0, & \text{otherwise (i.e., element } e_i \text{ is not connected to node } v_j). \end{cases} \tag{2}$$

Definition 4. The Kronecker product operator $\otimes$ is defined as

$$X \otimes Y : (\mathbb{R}^{n\times m}, \mathbb{R}^{r\times q}) \to \mathbb{R}^{nr\times mq}, \quad \text{where } [X \otimes Y]_{i,j\,\text{block}} = X_{ij} Y.$$

By construction one can show that the vector $\mathbf{g}(\mathbb{E}, \mathbb{P})$ can be defined as

$$\mathbf{g} = (M \otimes I_3)\mathbf{p} = \mathbf{M}\mathbf{p}, \quad \mathbf{M}(\mathbb{E}) = M(\mathbb{E}) \otimes I_3. \tag{3}$$

The sparse matrix $\mathbf{M} \in R^{3n_e \times 3n_n}$ appearing in this definition is called the *connectivity matrix*. In order to emphasize its dependence on the element set $\mathbb{E}$, the connectivity matrix will often be denoted by $\mathbf{M}(\mathbb{E})$. The matrix M will be called the *reduced* connectivity matrix since it completely defines how individual elements are connected in the overall structure.

If the n_s string elements in $\mathbb{E}_s$ appear first, then the vector $\mathbf{g}$ and matrix $\mathbf{M}$ can be partitioned in the form

$$\mathbf{g} = \begin{bmatrix} \mathbf{g}_s \\ \mathbf{g}_b \end{bmatrix} = \mathbf{M}\mathbf{p}, \;\; \mathbf{M} = \begin{bmatrix} \mathbf{S}^{\mathrm{T}} \\ \mathbf{B}^{\mathrm{T}} \end{bmatrix}, \quad \text{with } \mathbf{S} \in \mathbb{R}^{3n_n \times 3n_s}.$$

An important property of M used later in the text is given in the following theorem.

Theorem 1. *The reduced connectivity matrix satisfies the identity*

$$M\underline{\mathbf{1}}_{n_n} = 0, \quad \textit{where } \underline{\mathbf{1}}_{n_n} \in \mathbb{R}^{n_n} \textit{ is the vector of ones.}$$

Proof. All columns of M sum to zero since every row of M corresponds to exactly one element and has exactly two nonzero entries 1 and -1 corresponding to the starting and ending nodes. □

2.2. The tensegrity structure equilibrium conditions

If a structure with axially loaded elements is to be in prestressed equilibrium without any external forces, the internal element forces at each of the nodes must sum to zero.

Definition 5. The element force vector $\mathbf{f}_{ji} \in \mathbb{R}^3$ represents the contribution of the internal force of the element e_i to the balance of the forces at node v_j.

Since all elements of the structure are axially loaded, $\mathbf{f}_{ji}$ is collinear with the element vector $\mathbf{g}_i$. Note that $\mathbf{f}_{ji} \neq \mathbf{0}$ only if node v_j appears in the definition of the element e_i. Moreover, for any element $e_i = \{[v_j, v_k], z_i\}$ the element forces at the two opposite nodes v_j and v_k of the element satisfy $\mathbf{f}_{ji} = -\mathbf{f}_{ki}$. The magnitude of these forces is denoted by f_i.

We define a typical element c_{ji} of the matrix $C(\mathbb{E}) \in \mathbb{R}^{n_n \times n_e}$ as follows:

$$c_{ji} = \begin{cases} z_i, & \text{if } v_j \text{ is the first node of } e_i, \\ -z_i, & \text{if } v_j \text{ is the second node of } e_i, \\ 0, & \text{otherwise.} \end{cases} \tag{4}$$

With this definition it follows that

$$\mathbf{f}_{ji} = c_{ji}\lambda_i \mathbf{g}_i,$$

where λ_i scales the vector of the element so that it has the same magnitude as the collinear force vector. Note that λ_i represents the force per unit length of the element and will be called the *force-density*.

String elements are modeled as elements that can be either under tension or slack, but cannot be compressed. Since the force densities λ_i serve as variables in the problem, their positive values for the string elements preserve tensile character of the string forces. The force-density vector $\boldsymbol{\lambda} \in \mathbb{R}^{n_e}$ is defined by stacking force-densities of all elements in the single vector,

$$\boldsymbol{\lambda}^{\mathrm{T}} = [\,\lambda_1 \quad \lambda_2 \quad \cdots \quad \lambda_{n_e}\,], \quad \lambda_i \in \mathbb{R}.$$

If the structure is to be prestressed it is necessary to exclude the trivial solution $\boldsymbol{\lambda} = 0$. These undesirable solutions for the force-densities $\boldsymbol{\lambda}$, are eliminated by constraining the problem as follows:

$$\|\boldsymbol{\lambda}\| > 0, \tag{5}$$

$$\lambda_i \geqslant 0, \quad \text{for } e_i \in \mathbb{E}_s. \tag{6}$$

The balance of the forces at the node v_j can be written as

$$\sum_{i=1}^{n_e} \mathbf{f}_{ji} = \sum_{i=1}^{n_e} c_{ji}\lambda_i \mathbf{g}_i = 0. \tag{7}$$

Repeating this procedure for all nodes of the structure gives the set of equilibrium equations which can be written compactly as

$$\mathbf{C}\tilde{\mathbf{g}}\boldsymbol{\lambda} = 0, \tag{8}$$

where the linear operator $\tilde{\cdot}$ acting on the vector $\mathbf{x} \in \mathbb{R}^n_m$ is defined as follows,

$$\tilde{\mathbf{x}} := \mathrm{blockdiag}\{\mathbf{x}_1, \ldots, \mathbf{x}_i, \ldots, \mathbf{x}_n\} \in \mathbb{R}^{mn \times n}, \quad \mathbf{x}_i \in \mathbb{R}^m.$$

The sparse matrices $C(\mathbb{E})$ and $\mathbf{C}(\mathbb{E}) \in \mathbb{R}^{3n_n \times 3n_e}$ appearing in (8) satisfy $\mathbf{C} = C \otimes I_3$ and will be called the *reduced connectivity matrix* and *connectivity matrix* respectively. These matrices incorporate structure connectivity information analogous to M and $\mathbf{M}$. Moreover, it can be shown from (2) and (4) that

$$\mathbf{M} = \begin{bmatrix} \mathbf{S}^{\mathrm{T}} \\ \mathbf{B}^{\mathrm{T}} \end{bmatrix} \quad \text{and} \quad \mathbf{C} = [\,-\mathbf{S} \quad \mathbf{B}\,], \tag{9}$$

or, equivalently,

$$C = -M^{\mathrm{T}}\tilde{\mathbf{z}}, \quad \mathbf{C} = -\mathbf{M}^{\mathrm{T}}(\tilde{\mathbf{z}} \otimes I_3). \tag{10}$$

Note that (5), (6) and (8) represent necessary but not sufficient conditions for the existence of the equilibrium tensegrity structure. Solving (5), (6) and (8) for the variables $\mathbf{g}$ and $\boldsymbol{\lambda}$ may lead to the solution for which $\mathbf{g}$ does not represent a connected network of elements. The element vector definition (3), may be used as the change of variables to solve this problem.

Define the linear operator $\hat{(\cdot)}$ acting on the vector $\mathbf{x} \in \mathbb{R}^n$ by,

$$\hat{\mathbf{x}} := \tilde{\mathbf{x}} \otimes I_3 \in \mathbb{R}^{3n \times 3n}.$$

After some simple algebra, the identity (8) may be rewritten in the form,

$$\mathbf{C}\hat{\boldsymbol{\lambda}}\mathbf{g} = 0, \tag{11}$$

and the change of variables given in (3), yields,

$$\mathbf{C}\hat{\boldsymbol{\lambda}}\mathbf{M}\mathbf{p} = 0. \tag{12}$$

Finally, by including (5) and (6), we obtain the relations characterizing the most general tensegrity form-finding problem:

$$\mathbf{C}\hat{\boldsymbol{\lambda}}\mathbf{M}\mathbf{p} = 0, \tag{13}$$

$$\|\boldsymbol{\lambda}\| > 0, \tag{14}$$

$$\lambda_i \geqslant 0, \quad e_i \in \mathbb{E}_s. \tag{15}$$

Observe that any $\boldsymbol{\lambda}$ satisfying (13)–(15) in the nodal configuration $\mathbf{p}$ lies in the intersection of two convex sets. From (8), the first of these sets is the null space of the matrix $\mathbf{C}\tilde{\mathbf{g}}$. The second is the set of vectors $\boldsymbol{\lambda}$ satisfying $\lambda_i \geqslant 0$, $e_i \in \mathbb{E}_s$. Note that for any $\boldsymbol{\lambda}$ that satisfies (13)–(15), $a\boldsymbol{\lambda}$ also satisfies these equations if $a > 0$. Hence, the set of force-density vectors $\boldsymbol{\lambda}$ solving (13)–(15) in the nodal configuration $\mathbf{p}$ constitutes a convex cone.

Definition 6. Let

$$\Lambda \in \mathbb{R}^{n_e \times n_{pm}}, \quad \Lambda = \begin{bmatrix} \boldsymbol{\lambda}^1 & \boldsymbol{\lambda}^2 & \cdots & \boldsymbol{\lambda}^{n_{pm}} \end{bmatrix},$$

be the matrix with columns formed from of all n_{pm} linearly independent solutions $\boldsymbol{\lambda}^j$ of (13)–(15) in the nodal configuration $\mathbf{p}$. The *prestress cone* $\mathscr{C}(\Lambda)$, of the tensegrity structure in the nodal configuration $\mathbf{p}$, is the cone spanned by the linear combination of the columns of the matrix Λ, such that $\boldsymbol{\lambda} \in \mathscr{C}(\Lambda) \Rightarrow \lambda_i \geqslant 0$, $\forall e_i \in \mathbb{E}_s$. The linearly independent force-density vectors $\boldsymbol{\lambda}^j$ and n_{pm} are called respectively the *prestress modes* and the *number of prestress modes* of the tensegrity structure in the nodal configuration $\mathbf{p}$.

The tensegrity equilibrium equations imply that the triple $\Gamma = \{\mathbb{E}, \mathbb{P}, \Lambda\}$ completely defines the equilibrium of a tensegrity structure.

3. Shape constraints

In order to include different shape requirements it is necessary to add shape constraints to the problem. The general form of a shape constraint is:

$$\varphi(\mathbf{p}) = 0, \tag{16}$$

where φ is some general vector-valued function. Some common shape constraints are analyzed in more detail below.

3.1. Linear shape constraints

Certain shape constraints are linear in the nodal position vector $\mathbf{p}$. A constraint of this type requires that some nodes be located at specified positions; for example, some nodes of the tensegrity structure must be attached to supports. Another example occurs when some nodes must be located at certain positions to support external loads (see the left illustration of Fig. 1). This type of shape constraint may be written in the form

$$\mathbf{P}\mathbf{p} = \mathbf{p}_c, \tag{17}$$

where $\mathbf{p}_c$ is the given vector of specified positions and $\mathbf{P}$ is a sparse matrix of ones that extracts the constrained elements of $\mathbf{p}$.

If the desired shape has nodes lying on a flat surface, then the set of shape constraints also has a linear form similar to (17). Tensegrity plates are the class of tensegrity structures that have all nodes of the structure lying in two separated parallel planes. The tensegrity plate flatness constraint can be written as

$$\mathbf{n}^{\mathrm{T}}\mathbf{g}_i = 0, \quad e_i \in \mathbb{E}_h,$$

where $\mathbb{E}_h \in \mathbb{E}$ is the subset of the elements lying in the planes perpendicular to the vector $\mathbf{n} \in \mathbb{R}^3$ (see the right illustration of Fig. 1). When written in compact form, these constraints become

$$\begin{bmatrix} \mathbf{n}^{\mathrm{T}} & 0 & \dots & 0 \\ 0 & \mathbf{n}^{\mathrm{T}} & \dots & 0 \\ \vdots & \vdots & \ddots & \vdots \\ 0 & 0 & \dots & \mathbf{n}^{\mathrm{T}} \end{bmatrix} \mathbf{H}\mathbf{M}\mathbf{p} = (I \otimes \mathbf{n}^{\mathrm{T}})\mathbf{H}\mathbf{M}\mathbf{p},$$

where $\mathbf{H}$ is the sparse matrix that extracts the entries of $\mathbf{g}$ associated with the elements $\mathbb{E}_h$.

3.2. Constraints on the element length

The constraint that n_c elements must have predefined lengths is defined as,

$$\|\mathbf{g}_i\| = l_{c_i}, \quad e_i \in \mathbb{E}_{lc}, \tag{18}$$

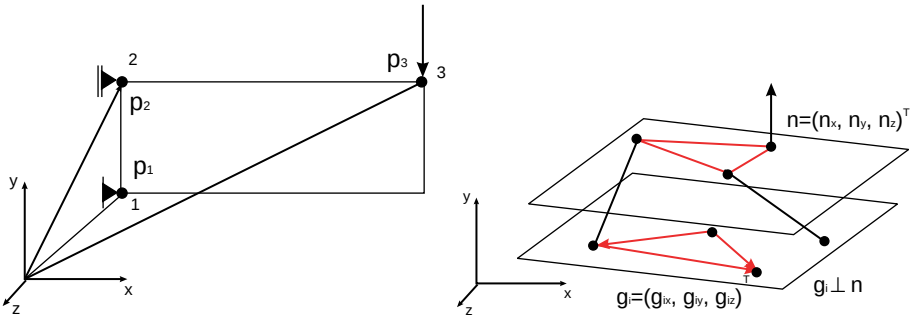

Fig. 1. Node and plate constraint.

where $\mathbb{E}_{lc} \in \mathbb{E}$ is the subset of elements with constrained lengths, and $\mathbf{l}_c \in \mathbb{R}^{n_c}$ is a given vector. By its nature this constraint is quadratic,

$$\tilde{\mathbf{g}}_c^{\mathrm{T}} \mathbf{g}_c = \tilde{\mathbf{l}}_c \mathbf{l}_c, \quad \mathbf{l}_c^{\mathrm{T}} = \begin{bmatrix} l_{c_1} & l_{c_2} & \cdots & l_{c_{n_e}} \end{bmatrix}, \tag{19}$$

where $\mathbf{g}_c \in \mathbb{R}^{n_c}_3$ is the vector formed by collecting the element vectors of the elements in $\mathbb{E}_{lc}$.

3.3. Symmetric tensegrity structures

In many practical situations tensegrity structures and their desired shapes are symmetric. In this case, the amount of information required to describe the geometry and element forces can be significantly reduced. Two examples of symmetric structures are shown in Figs. 2 and 3.

Definition 7. A *symmetry* of a set S is an isometry that maps S onto itself (see, e.g., Grunbaum and Shepard, 1986).

Isometries are bijective mappings that preserve distances between points and angles between lines in the set. Symmetries associated with tensegrity structures that are of relevance for form-finding problems can be divided in two groups, nodal symmetry and element symmetry.

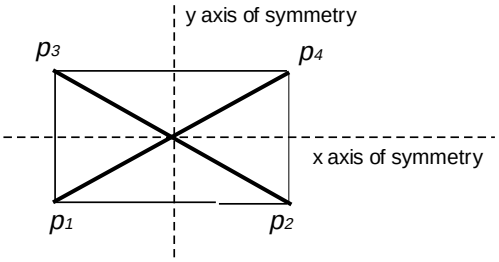

Fig. 2. A tensegrity cross that admits symmetries with respect to the x and y-axis.

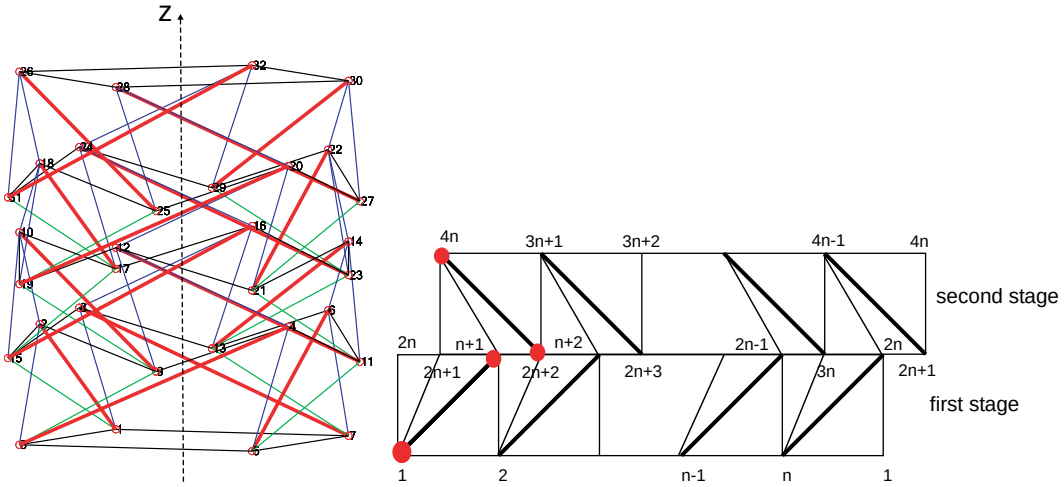

Fig. 3. The left figure is a Class 1 shell-class tensegrity tower that admits symmetries about z-axis; the right figure is a connectivity diagram of a shell-class tensegrity.

3.3.1. Nodal symmetry

The set of nodal vectors $\mathbb{P}$ of a tensegrity structure and any subset $\mathbb{P}_s \in \mathbb{P}$ are subsets of the Euclidian space $\mathbb{R}^3$. It can be shown that all symmetries (i.e., isometries) $\mathscr{I}(\mathbf{p}_k)$, $\mathbf{p}_k \in \mathbb{R}^3$, are affine mappings of the form

$$\mathscr{I}(\mathbf{p}_k) = \mathbf{p}_j = R\mathbf{p}_k + \mathbf{t}, \quad R \in \mathbb{R}^{3\times 3}, \ RR^{\mathrm{T}} = R^{\mathrm{T}}R = I_3, \ \mathbf{t} \in \mathbb{R}^3. \tag{20}$$

Definition 8. A subset of nodes $\mathbb{N}_s \in \mathbb{N}$ of a tensegrity structure is said to admit *nodal symmetry* $\mathscr{I}$ if the associated set of nodal vectors $\mathbb{P}_s \in \mathbb{P}$ satisfies (20) for some R and $\mathbf{t}$. If the set $\mathbb{N}_s$ involves all nodes of $\mathbb{N}$, i.e., $\mathbb{N}_s = \mathbb{N}$, then the tensegrity structure is said to have *compete nodal symmetry*.

The structure in Fig. 2 admits a nodal symmetry since rotation about the y-axis yields,

$$\mathbf{p}_2 = R\mathbf{p}_1 + \mathbf{t}, \quad \mathbf{p}_1 = R\mathbf{p}_2 + \mathbf{t}, \quad \mathbf{p}_4 = R\mathbf{p}_3 + \mathbf{t}, \quad \mathbf{p}_3 = R\mathbf{p}_4 + \mathbf{t},$$

$$R = \begin{bmatrix} -1 & 0 & 0 \\ 0 & 1 & 0 \\ 0 & 0 & 1 \end{bmatrix} \quad \text{and} \quad \mathbf{t} = 0.$$

3.3.2. Element symmetry

According to Definition 2, elements $e_i \in \mathbb{E}$ of a tensegrity structure are not vectors in Euclidian space. Hence, the idea of element symmetry is different from that of nodal symmetry.

Definition 9. A subset of elements $\mathbb{E}_s \in \mathbb{E}$ of a tensegrity structure is said to admit *element symmetry* $\mathscr{I}$ if:

(i) the set of nodes $\mathbb{N}_s = \mathbb{N}(\mathbb{E}_s)$, defining the elements $\mathbb{E}_s$, admits nodal symmetry $\mathscr{I}$;
(ii) for every element $e_i = \{[v_j, v_k], z_i\} \in \mathbb{E}_s$ there exists exactly one element $e_q = \{[v_r, v_s], z_q\} \in \mathbb{E}_s$, such that $\mathbf{p}_r = \mathscr{I}(\mathbf{p}_j)$, $\mathbf{p}_s = \mathscr{I}(\mathbf{p}_k)$, or $\mathbf{p}_r = \mathscr{I}(\mathbf{p}_k)$, $\mathbf{p}_s = \mathscr{I}(\mathbf{p}_j)$; and
(iii) $z_i = z_q$.

If the set $\mathbb{E}_s$ involves all elements of $\mathbb{E}$, i.e., $\mathbb{E}_s = \mathbb{E}$, then the tensegrity structure is said to have *complete element symmetry*.

Definition 10. Two elements e_i and e_q of the same kind or two nodes v_j and v_r are said to be equivalent, or to belong to the same *equivalency class* $\mathbb{E}_{ec} \in \mathbb{E}$, and $\mathbb{N}_{ec} \in \mathbb{N}$ respectively, if there exist a complete element symmetry or a complete nodal symmetry that maps one to the other.

Other symmetries can be associated with a tensegrity structure, such as deformation symmetry and applied force symmetry. However, these symmetries have no relevance for form-finding and are not considered in this paper.

3.3.3. Complete element symmetry and the reduction of force-density variables

Complete element symmetry can be exploited to reduce the number of variables in the tensegrity equilibrium equations. The main result that establishes the basis for this claim is given in Theorem 2. The next two lemmas establish some background results.

Lemma 1. *If a finite or infinite tensegrity structure admits complete element symmetry* $\mathscr{I}(\mathbf{x}) = R\mathbf{x} + \mathbf{t}$, *then any mapping between element vectors,* $\mathbf{g}_i$ *and* $\mathbf{g}_q$ *associated with any two elements* e_i *and* e_q *in the same equivalency class, must be strictly linear and satisfy the relations*

$$\mathbf{g}_q = R\mathbf{g}_i, \quad \textit{or} \quad \mathbf{g}_q = -R\mathbf{g}_i. \tag{21}$$

Proof. Without loss of generality we assume the element vector orientation $\mathbf{g}_i = \mathbf{p}_k - \mathbf{p}_j$ and $\mathbf{g}_q = p_r - \mathbf{p}_s$. From Definition 9 (ii),

$$\mathbf{p}_r = R\mathbf{p}_k + \mathbf{t}, \quad \mathbf{p}_s = R\mathbf{p}_j + \mathbf{t}, \quad \text{or} \quad \mathbf{p}_r = R\mathbf{p}_j + \mathbf{t}, \quad \mathbf{p}_s = R\mathbf{p}_k + \mathbf{t}.$$

It follows that $\mathbf{g}_q$ must satisfy one of the two conditions,

$$\mathbf{g}_q = \mathbf{p}_r - \mathbf{p}_s = (R\mathbf{p}_k + \mathbf{t} - R\mathbf{p}_j - \mathbf{t}) = R(\mathbf{p}_k - \mathbf{p}_j) = R\mathbf{g}_i, \tag{22}$$

or

$$\mathbf{g}_q = \mathbf{p}_r - \mathbf{p}_s = (R\mathbf{p}_j + \mathbf{t} - R\mathbf{p}_k - \mathbf{t}) = R(\mathbf{p}_j - \mathbf{p}_k) = -R\mathbf{g}_i. \qquad \square \tag{23}$$

Note that although a structure may admit element symmetry, the set of element vectors $\mathbf{g}$ does not necessarily admit the same symmetry, or even any symmetry at all. This is because the definition of the element vectors depends on their adopted orientation. If the orientation of the element vectors does not comply with the symmetry of the structure, then the set of element vectors may not be symmetric. Nonetheless, Lemma 1 shows that the mappings between the element vectors of the elements in the same element equivalency class are not independent of the symmetry.

The next lemma shows that the contributions of the element forces of two elements in the same equivalency class at two nodes in the same equivalency class are related by a symmetry mapping that is independent of the adopted orientation of the element vectors.

Lemma 2. *Let a finite or infinite tensegrity structure admit complete element symmetry* $\mathscr{I}(\mathbf{x}) = R(\mathbf{x}) + \mathbf{t}$, *and let* v_j *and* v_r *be any two nodes in the same node equivalency class. Then for any element* e_q *connected to node* v_r, *it holds that*

(i) *there exists exactly one element* e_i (*not necessarily different from* e_q) *connected to node* v_j, *that is in the same equivalency class*; *and*
(ii) *the compressive or tensional character of the element force is preserved under the symmetry transformation i.e.*,

$$c_{rq}\mathbf{g}_q = c_{ji}R\mathbf{g}_i. \tag{24}$$

Proof. Since nodes v_j and v_r are in the same equivalency class, Definition 9 implies that for every element incident with node v_j there must be at least one element in the same equivalency class that is incident with node v_r . This result, and the fact that symmetries are bijective mappings implies (i).

Without loss of generality we assume that $e_i = \{[v_j, v_k], z_i\}$ and $\mathbf{g}_i = \mathbf{p}_k - \mathbf{p}_j$. There are two possible cases. First, assume that the orientation of the element e_q is such that $e_q = \{[v_r, v_s], z_q\}$. Then from (4), $c_{ji} = c_{ri}$ since from Definition 9 (iii), $z_i = z_q$. In this case (22) holds, so that $\mathbf{g}_q = R\mathbf{g}_i$. Finally, we have that

$$c_{rq}\mathbf{g}_q = c_{ji}R\mathbf{g}_i.$$

In the second case the orientation of the element e_q is such that $e_q = \{[v_s, v_r], z_q\}$. From (4) it must hold that $c_{rq} = -c_{ji}$. Hence, from (23) we have $\mathbf{g}_q = -R\mathbf{g}_i$, and it follows that

$$c_{rq}\mathbf{g}_q = (-c_{ji})(-R\mathbf{g}_i) = c_{ji}R\mathbf{g}_i. \qquad \square$$

Theorem 2. *Suppose a tensegrity structure admits a complete element symmetry. Then the tensegrity equilibrium equations (13)–(15) are satisfied if all elements in the same element equivalency class $\mathbb{E}_{ec}^{k}$ have a common force-density*,

$$\lambda_i = \lambda_j, \quad \forall e_i, e_j \in \mathbb{E}_{ec}^{k}.$$

Proof. Let v_j and v_r be two nodes in the same node equivalency class. The equilibrium equations at nodes v_j and v_r are given by,

$$\sum_{i=1}^{n_e} c_{ji}\lambda_i \mathbf{g}_i = \sum_{i\in\mathbb{I}_j} c_{ji}\lambda_i \mathbf{g}_i = 0, \tag{25}$$

$$\sum_{i=1}^{n_e} c_{rq}\lambda_q \mathbf{g}_q = \sum_{q\in\mathbb{I}_r} c_{rq}\lambda_q \mathbf{g}_q = 0, \tag{26}$$

where $\mathbb{I}_j$ and $\mathbb{I}_r$ are the sets of indices of the elements incident with nodes v_j and v_r. Let the notation $\lambda_q = \lambda_q(i)$ indicate the dependence of the force-density λ_q on λ_i. Using (24), every term $c_{rq}\lambda_q \mathbf{g}_q$ in the summation (26) can be substituted with exactly one term $c_{ji}\lambda_q(i)R\mathbf{g}_i$. After changing the indexing of the summation (26), it follows that the balance of forces at the node v_r can be written as

$$\sum_{i\in\mathbb{I}_j} c_{ji}\lambda_q(i)R\mathbf{g}_i = 0. \tag{27}$$

Pulling out matrix R from the summation gives,

$$R\sum_{i\in\mathbb{I}_j} c_{ji}\lambda_q(i)\mathbf{g}_i = 0. \tag{28}$$

If $\lambda_q(i)$ is chosen so that $\lambda_q(i) = \lambda_i$, i.e., if $\lambda_q = \lambda_i$, then (28) can be rewritten as

$$R\sum_{i\in\mathbb{I}_j} c_{ji}\lambda_i \mathbf{g}_i = 0,$$

which always holds when (25) holds. □

Note that $\lambda_q(i) = \lambda_i$ is a sufficient but not necessary condition for equilibrium at node v_r. To illustrate this point, note that the symmetric tensegrity structure of Fig. 4, with connectivity defined in Fig. 5, admits both a symmetric and an asymmetric solution for $\boldsymbol{\lambda}$. The difference in the two examples is only in the distribution of the resulting element forces. The left structure in Fig. 4 has the same force-density for the symmetric elements, while the right structure does not. This example shows that the result of Hinrichs (1984) used by Connelly and Terrell (1995) for analysis of tensegrity prisms, which states that these structures with the least number of strings admit only symmetric prestress, does not necessarily apply to all symmetric tensegrities.

Let all elements $\mathbb{E}$ of the structure that admits a complete element symmetry, be grouped in n_{ec} disjoint element equivalency classes $\mathbb{E}_{ec}^{j}, j = 1,\ldots,n_{ec}$. Theorem 2 can be used to reduce the number of force-density variables from $\boldsymbol{\lambda} \in \mathbb{R}^{n_e}$ to $\underline{\boldsymbol{\lambda}} \in \mathbb{R}^{n_{ec}}$, where $\underline{\boldsymbol{\lambda}}$ is the reduced force-density vector formed from the single representative elements for each equivalency class $\mathbb{E}_{ec}^{j}$. The *element equivalency class incidence matrix* $Q \in \mathbb{R}^{n_e \times n_{ec}}$, has elements q_{ij} defined as follows:

$$q_{ij} = \begin{cases} 1, & \text{if } e_i \in \mathbb{E}_{ec}^{j}, \\ 0, & \text{otherwise.} \end{cases} \tag{29}$$

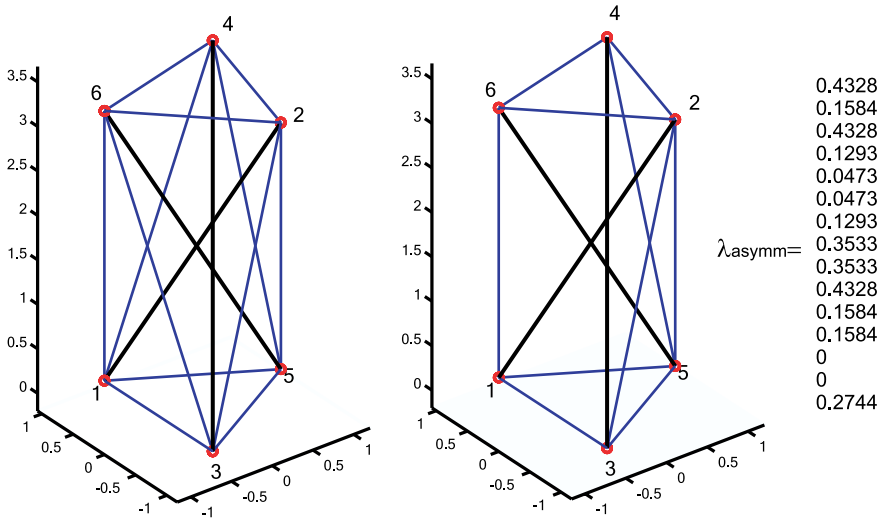

Fig. 4. Left: Symmetric distribution of the prestress in the three-bar structure in the configuration with the relative angle between top and bottom triangles $\pi/4$. Right: Elements with nonzero prestress of the same structure with asymmetric distribution of prestress.

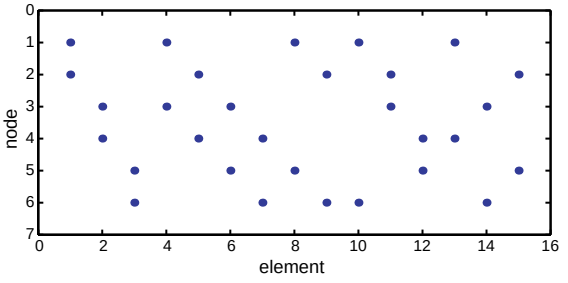

Fig. 5. Connectivity matrix of the three bar structure.

Given Q, the reduction in the number of variables can be written as

$$\boldsymbol{\lambda} = Q\underline{\boldsymbol{\lambda}}. \tag{30}$$

3.3.4. Complete element symmetry and reduction of the number of equilibrium equations

Recall that complete element symmetry implies complete nodal symmetry of a tensegrity structure. Hence, the set of all nodes $\mathbb{N}$ can be partitioned in n_{nc} disjoint node equivalency classes $\mathbb{N}^i_{ec}$, $i = 1, \ldots, n_{nc}$. As suggested by (28), equilibrium conditions for any two nodes in the same equivalency class become linearly dependant and are related via the nonsingular linear transformation R. This redundancy can be exploited further to reduce the number of equilibrium equations in (13) by keeping only the set of independent equations at the single representative nodes for each node equivalency class $\mathbb{N}^i_{ec}$. Let d_{ij} denote the elements a matrix $D \in \mathbb{R}^{n_{nc} \times n_n}$ such that

$$d_{ij} = \begin{cases} 1, & \text{if node } v_j \text{ is the representative node of } \mathbb{N}^i_{ec}, \\ 0, & \text{otherwise.} \end{cases}$$

The reduction in the number of equations can be represented by pre-multiplying (13) by the matrix $\mathbf{D} \in R^{3n_{nc} \times 3n_n}$, where $\mathbf{D} = D \otimes I_3$.

3.3.5. Nodal symmetry and reduction of the number of geometric variables

The fact that a tensegrity structure admits nodal symmetry can be used to reduce the number of geometric variables $\mathbf{p}$ in the tensegrity equilibrium equations. Let a tensegrity structure have n_{nc} different node equivalency classes $\mathbb{N}^i_{nc}$. Then, for any two nodes v_j and v_r in the same equivalency class $\mathbb{N}^i_{nc}$, there exists a symmetry mapping such that,

$$\mathbf{p}_r = R_{rj}\mathbf{p}_j, \quad R_{rj} \in \mathbb{R}^{3\times 3}. \tag{31}$$

Let the node v_j be selected to be the representative node for the node equivalency class $\mathbb{N}^i_{nc}$. Since all nodes in the node equivalency class $\mathbb{N}^i_{nc}$ are images of the representative node v_j, by using (31) for each of the n_{nc} node equivalency classes, it is possible to write,

$$\mathbf{p} = \mathscr{R}\underline{\mathbf{p}}, \text{ for } \mathscr{R} \in \mathbb{R}^{3n_n \times 3n_{nc}} \quad \text{and} \quad \underline{\mathbf{p}} \in \mathbb{R}^{n_{nc}}_3. \tag{32}$$

The vector $\underline{\mathbf{p}}$ is formed by collecting all nodal vectors of the representative nodes for each of the n_{nc} different node equivalency classes. Fig. 3 depicts the nodes with nodal vectors forming $\underline{\mathbf{p}}$ for the shell-class tensegrity structures defined in Skelton et al. (2001).

Eq. (32) provides the change of variables that reduces the number of geometric variables $\mathbf{p}$ in (13) and (14) from $3n_n$ to $3n_{nc}$. This change of variables guarantees nodal symmetry of the solution and simultaneously preserves the bilinear character of the tensegrity equilibrium equations. In summary, the form of the tensegrity equilibrium equations that accommodates both nodal symmetry and element symmetry of the tensegrity structure can be written in the form:

$$\mathbf{D}\mathbf{C}\widehat{Q\underline{\boldsymbol{\lambda}}}\mathscr{R}\underline{\mathbf{p}} = 0, \tag{33}$$

$$\|\underline{\boldsymbol{\lambda}}\| > 0, \tag{34}$$

$$\underline{\lambda}_i \geqslant 0, \quad e_i \in \underline{\mathbb{E}}_s. \tag{35}$$

3.4. Symmetric tensegrities and parametrization of geometry

The complexity of the tensegrity form-finding problem is influenced by the complexity of both the tensegrity equilibrium equations and the shape constraints. Although the tensegrity equilibrium equations have the nice bilinear form when the nodal vector $\mathbf{p}$ is used to describe the geometry, a sensible change of variables may yield more tractable equations and hence improve the convergence of algorithms used to solve them.

The cylindrical shell-class tensegrity structure in Fig. 3 is analyzed to illustrate this fact. Given n-bars per stage, this structure admits rotations by $2k\pi/n$, $k = i, \ldots, n-1$ about z axis, as the element symmetries. The geometry constraint that requires all nodes to lie on the cylinder of radius r_{target} has the quadratic form

$$p^2_{i_x} + p^2_{i_y} = r^2_{\text{target}}, \quad i = 1, \ldots, n_{nc}.$$

If r is a geometric variable, this constraint is linear, i.e., $r = r_{\text{target}}$. In some cases, it is beneficial to find a set of geometric variables for which the equilibrium Eq. (13) becomes more nonlinear, but the additional shape constraints are less nonlinear. The next section addresses this issue for shell-class tensegrity structures.

3.4.1. Geometry parametrization of a symmetric shell-class tensegrity tower

This class of tensegrity structure has n bars for each of the n_{st} stages (see Figs. 3 and 6). In addition to the rotational symmetry about the z axis, a structure may also admit other symmetries—for example, reflection about the plane perpendicular to the axis passing through the middle of the height of the structure.

For each of n_{st} stages, let l_{b_i} denote the length of the bars, r_i the radius of the bottom polygon, and α_i the twist angle, as shown in Fig. 6. Let the truncation ratio of the stages be defined as

$$t_i = \frac{r_i^t}{r_i}, \quad i = 1, \ldots, n_{st},$$

where r_i^t, $i = 1, \ldots, n_{st}$ are the radii of the top polygons of the stages. Similarly, let β_i, $i = 1, \ldots, n_{st} - 1$, and γ_i, $i = 1, \ldots, n_{st} - 1$ denote the parameters that define the positions of the stages relative to each other, as depicted in Fig. 6. We define the collections of geometric parameters: $\mathbf{l}_b \in \mathbb{R}^{n_{st}}$, $\mathbf{r} \in \mathbb{R}^{n_{st}}$, $\mathbf{t} \in \mathbb{R}^{n_{st}}$, $\boldsymbol{\alpha} \in \mathbb{R}^{n_{st}}$, $\boldsymbol{\gamma} \in \mathbb{R}^{n_{st}-1}$ and $\boldsymbol{\beta} \in \mathbb{R}^{n_{st}-1}$.

Let $\mathbf{p}_{ji}^b$ denote the nodal vectors of the $j = 1, \ldots, n$ nodes at the bottom of each of the $i = 1, \ldots, n_{st}$ stages. Similarly, let $\mathbf{p}_{ji}^t$ denote the nodal vectors of the $j = 1, \ldots, n$ nodes at the top of each of the $i = 1, \ldots, n_{st}$ stages. Finally, we define the orthogonal rotation matrix about z-axis:

$$R(x) = \begin{bmatrix} \cos x & \sin x & 0 \\ -\sin x & \cos x & 0 \\ 0 & 0 & 1 \end{bmatrix}.$$

With these definitions, the geometry of a symmetric shell-class tensegrity can be parameterized as follows:

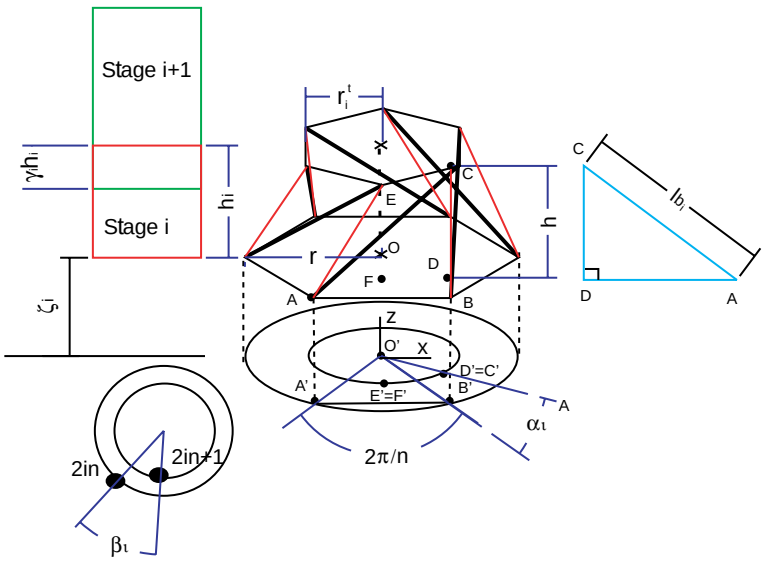

Fig. 6. Geometric parameters of a stage of a shell-class tensegrity.

$$
\begin{aligned}
&\mathbf{p}_{ji}^{b} = R\left((j-1)\frac{2\pi}{n}\right)\mathbf{p}_{1,i}^{b}, \quad \mathbf{p}_{ji}^{t} = R\left((j-1)\frac{2\pi}{n}\right)\mathbf{p}_{1,i}^{t},\\
&\mathbf{p}_{1,i}^{b} = R(\delta_i^b)\begin{bmatrix} r_i \\ 0 \\ \zeta_i \end{bmatrix}, \quad \mathbf{p}_{1,i}^{t} = R(\delta_i^t)\begin{bmatrix} t_i r_i \\ 0 \\ \zeta_i + h_i \end{bmatrix},\\
&\delta_1^b = 0, \quad \delta_i^b = \delta_{i-1}^b + (-1)^i\left(\alpha_{i-1} + \beta_{i-1} + \frac{2\pi}{n}\right),\\
&\delta_i^t = \delta_i^b + (-1)^{i-1}\left(\alpha_i + \frac{2\pi}{n}\right),\\
&\zeta_1 = 0, \quad \zeta_i = \zeta_{i-1} + (1-\gamma_i)h_i,\\
&h_i = \sqrt{l_{b_i}^2 - r_i^2 - t^2 r_i^2 + 2r_i^2 t\cos\left(\frac{2\pi}{n} + \alpha_i\right)},
\end{aligned}
\tag{36}
$$

where δ_i^b and δ_i^t are the angular coordinates of the nodes at $\mathbf{p}_{ji}^b$ and $\mathbf{p}_{ji}^t$ respectively, and h_i is the height of the stages $i = 1,\ldots,n_{st}$.

Note that all nodes $\mathbf{p}_{ji}^b$ in the same stage $i = 1,\ldots,n_{st}$ belong to the same node equivalency class. Similarly, all nodes $\mathbf{p}_{ji}^t$, $i = 1,\ldots,n_{st}$, in the same stage $i = 1,\ldots,n_{st}$ belong to the same node equivalency class. Suppose that the nodes $\mathbf{p}_{1,i}^b$ and $\mathbf{p}_{1,i}^t$, $i = 1,\ldots,n_{st}$, are selected as the representative nodes for the $2n_{st}$ different node equivalency classes. Using these nodes to form the vector $\underline{\mathbf{p}} \in \mathbb{R}_3^{2n_{st}}$, the geometry parametrization (36) can be written in the compact form

$$
\mathbf{p} = \mathscr{R}\underline{\mathbf{p}}, \quad \text{with } \underline{\mathbf{p}} = \underline{\mathbf{p}}(n, \mathbf{l}_b, \mathbf{r}, \mathbf{t}, \boldsymbol{\alpha}, \boldsymbol{\beta}, \boldsymbol{\gamma}). \tag{37}
$$

4. Invariant tensegrity geometric transformations

In this section it will be shown that Theorem 2 is a special case of a more general property of tensegrity structures.

Definition 11. Suppose that the geometry of the equilibrium tensegrity structure $\Gamma = \{\mathbb{E}, \mathbf{p}, \Lambda\}$ is transformed using $\bar{\mathbf{p}} = T(\mathbf{p})$. If the transformed structure $\overline{\Gamma} = \{\mathbb{E}, \bar{\mathbf{p}}, \Lambda\}$ is in equilibrium, then T is known as an *invariant tensegrity geometric transformation*.

Theorem 3. *Any affine geometric transformation of the nodal position vector* $\mathbf{p}$ *of the form* $\bar{\mathbf{p}} = \mathscr{A}\mathbf{p} + \mathscr{T}$, *where*,

$$
\mathscr{A} \in \mathbb{R}^{3n_n \times 3n_n}, \quad \mathscr{A} = I_{n_n} \otimes A, \ A \in \mathbb{R}^{3\times 3},
$$

$$
\mathscr{T} = \underline{\mathbf{1}}_{n_n} \otimes \mathbf{t} = (\underline{\mathbf{1}}_{n_n} \otimes I_3)\mathbf{t}, \quad \mathbf{t} \in \mathbb{R}^3,
$$

is an invariant tensegrity geometric transformation. The affine geometric transformation is known as the tensegrity similarity transformation.

Proof. Since $\Gamma = \{\mathbb{E}, \mathbf{p}, \Lambda\}$ is an equilibrium tensegrity structure, it satisfies the tensegrity equilibrium equation:

$$
\mathbf{C}\hat{\boldsymbol{\lambda}}\mathbf{M}\mathbf{p} = 0. \tag{38}
$$

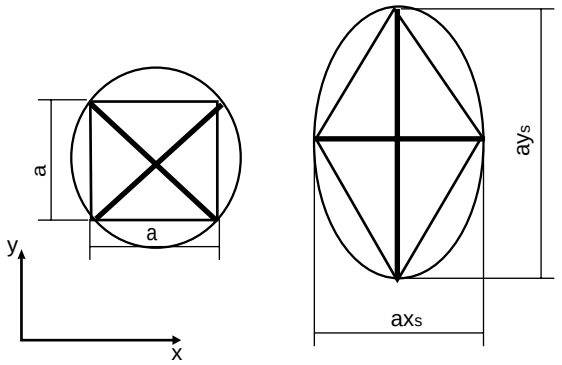

Fig. 7. An equilibrium elliptical tensegrity cross generated by the similarity transformation from the equilibrium square configuration.

Equilibrium of the structure $\overline{T} = \{\mathbb{E}, I(\mathbf{p}), \Lambda\}$ is satisfied if:

$$\mathbf{C}\hat{\boldsymbol{\lambda}}\mathbf{M}\big((I_{n_n} \otimes A)\mathbf{p} + (\underline{\mathbf{1}}_{n_n} \otimes I_3)\mathbf{t}\big) = \mathbf{C}\hat{\boldsymbol{\lambda}}\mathbf{M}(I_{n_n} \otimes A)\mathbf{p} + \mathbf{C}\hat{\hat{\boldsymbol{\lambda}}}\mathbf{M}(\underline{\mathbf{1}}_{n_n} \otimes I_3)\mathbf{t}.$$

Using the identity $\mathbf{M}(\underline{\mathbf{1}}_{n_n} \otimes I_3)\mathbf{t} = 0$ from Theorem 1, we obtain

$$\mathbf{C}\hat{\boldsymbol{\lambda}}\mathbf{M}\big((I_{n_n} \otimes A)\mathbf{p} + (\underline{\mathbf{1}}_{n_n} \otimes I_3)\mathbf{t}\big) = \mathbf{C}\hat{\boldsymbol{\lambda}}\mathbf{M}(I_{n_n} \otimes A)\mathbf{p}. \tag{39}$$

Rearranging this equation and applying (38) yields

$$\mathbf{C}\hat{\boldsymbol{\lambda}}\mathbf{M}(I_{n_n} \otimes A)\mathbf{p} = (I_{n_n} \otimes A)\mathbf{C}\hat{\boldsymbol{\lambda}}\mathbf{M}\mathbf{p} = 0. \qquad \square$$

Theorem 3 represents a powerful tool for the equilibrium analysis of tensegrity structures. It allows the trivial equilibrium analysis of all tensegrity structures with geometry defined via an affine transformation of a tensegrity structure with known equilibrium geometry. For example, it is possible to compute the equilibrium conditions for the tensegrity cross in Fig. 7 that has nodes at the vertices of a square. In this case, the equilibrium of any tensegrity cross with its nodes lying on an ellipse is guaranteed for the same set of force-densities of the corresponding elements. Note that the higher level of symmetry in the square tensegrity cross makes the number of geometric variables and the number of equilibrium equations smaller, thereby making the problem easier to solve. The linear part of the affine node position transformation that generates the equilibrium configuration of the elliptical cross is given by

$$A = \begin{bmatrix} x_s & 0 & 0 \\ 0 & y_s & 0 \\ 0 & 0 & 0 \end{bmatrix} R\left(\frac{\pi}{4}\right).$$

Although it is intuitively obvious that a tensegrity structure remains in equilibrium if it undergoes a geometric transformation as a rigid body (i.e., rotation or translation) it is not obvious that the same holds true for other affine transformations.

5. Stiffness matrix of a tensegrity structure

In the above analysis the necessary conditions are defined for the existence of a prestressed structure that satisfies the tensegrity conditions. The stability of a tensegrity structure can be examined by analyzing the properties of its stiffness matrix. In the next section the stiffness matrix of a tensegrity structure is defined. Since a tensegrity structure can be regarded as a special case of truss structures, the results are also applicable to these kinds of structures.

Definition 12. The *stiffness matrix* $\mathscr{K}$ of a tensegrity structure under the equilibrium external load $\mathbf{w} \in \mathbb{R}_3^{n_n}$ that acts at the nodes in the equilibrium nodal configuration $\mathbf{p}$ is defined as

$$\mathscr{K} = \frac{\partial \mathbf{w}}{\partial \mathbf{p}}.$$

One can show that the equilibrium conditions of a loaded structure can be written in a form similar to (13), i.e.

$$\mathbf{C}\hat{\boldsymbol{\lambda}}\mathbf{M}\mathbf{p} + \mathbf{w} = 0, \quad \text{with } \mathbf{w}^{\mathrm{T}} = \begin{bmatrix} \mathbf{w}_1^{\mathrm{T}} & \mathbf{w}_2^{\mathrm{T}} & \cdots & \mathbf{w}_{n_n}^{\mathrm{T}} \end{bmatrix}. \tag{40}$$

This establishes an equivalent definition of the stiffness matrix,

$$\mathscr{K} = -\frac{\partial}{\partial \mathbf{p}}(\mathbf{C}\hat{\boldsymbol{\lambda}}\mathbf{M}\mathbf{p}),$$

which we use in its derivation to get,

$$\mathscr{K} = -\frac{\partial}{\partial \boldsymbol{\lambda}}(\mathbf{C}\hat{\boldsymbol{\lambda}}\mathbf{M}\mathbf{p})\frac{\partial \boldsymbol{\lambda}}{\partial \mathbf{p}} - \mathbf{C}\hat{\boldsymbol{\lambda}}\mathbf{M}.$$

The first term of this expression can be more conveniently written for differentiating with respect to the vector $\boldsymbol{\lambda}$, which gives

$$\mathscr{K} = -\frac{\partial}{\partial \boldsymbol{\lambda}}(\mathbf{C}\tilde{\mathbf{g}}\boldsymbol{\lambda})\frac{\partial \boldsymbol{\lambda}}{\partial \mathbf{p}} - \mathbf{C}\hat{\boldsymbol{\lambda}}\mathbf{M} = -\mathbf{C}\tilde{\mathbf{g}}\frac{\partial \boldsymbol{\lambda}}{\partial \mathbf{p}} - \mathbf{C}\hat{\boldsymbol{\lambda}}\mathbf{M}.$$

The rest of the derivation of the stiffness matrix is completed assuming that elements are constructed from linear elastic materials that obey Hooke's law. If Young's modulus of the element e_i is denoted y_i, and its cross-sectional area and rest-length, a_i, and l_{0_i}, then the force-densities λ_i can be defined as,

$$\lambda_i = z_i \frac{y_i a_i}{l_{0i}\|\mathbf{g}_i\|}(\|\mathbf{g}_i\| - l_{0i}), \tag{41}$$

or equivalently,

$$\lambda_i = z_i \frac{y_i a_i}{l_{0i}}\left(1 - \frac{l_{0i}}{\|\mathbf{g}_i\|}\right). \tag{42}$$

Differentiation of $\boldsymbol{\lambda}$ with respect to $\mathbf{p}$ using (3) gives

$$\frac{\partial \boldsymbol{\lambda}}{\partial \mathbf{p}} = \frac{\partial \boldsymbol{\lambda}}{\partial \mathbf{g}}\frac{\partial \mathbf{g}}{\partial \mathbf{p}} = \frac{\partial \boldsymbol{\lambda}}{\partial \mathbf{g}}\mathbf{M}.$$

The relationship in (42) is used to get,

$$\frac{\partial \boldsymbol{\lambda}}{\partial \mathbf{g}} = \begin{bmatrix} z_1 y_1 a_1 \dfrac{\mathbf{g}_1^{\mathrm{T}}}{\|\mathbf{g}_1\|^3} & 0 & \cdots & 0 \\ 0 & z_2 y_2 a_2 \dfrac{\mathbf{g}_2^{\mathrm{T}}}{\|\mathbf{g}_2\|^3} & \cdots & 0 \\ \vdots & \vdots & \ddots & \vdots \\ 0 & 0 & \cdots & z_{n_e} y_{n_e} a_{n_e} \dfrac{\mathbf{g}_{n_e}^{\mathrm{T}}}{\|\mathbf{g}_{n_e}\|^3} \end{bmatrix}. \tag{43}$$

Defining the auxiliary vectors,

$$\mathbf{y} = [y_1, y_2, \ldots, y_{n_e}]^{\mathrm{T}}, \quad \mathbf{a} = [a_1, a_2, \ldots, a_{n_e}]^{\mathrm{T}}, \quad \mathbf{l} = [l_1, l_2, \ldots, l_{n_e}]^{\mathrm{T}},$$

allows us to write (43) in the compact form

$$\frac{\partial \boldsymbol{\lambda}}{\partial \mathbf{g}} = \tilde{\mathbf{z}}\tilde{\mathbf{y}}\tilde{\mathbf{a}}\tilde{\mathbf{l}}^{-3}\tilde{\mathbf{g}}^{\mathrm{T}}.$$

Substituting this derivative in the expression for $\partial\boldsymbol{\lambda}/\partial\mathbf{p}$ gives

$$\frac{\partial \boldsymbol{\lambda}}{\partial \mathbf{p}} = \tilde{\mathbf{z}}\tilde{\mathbf{y}}\tilde{\mathbf{a}}\tilde{\mathbf{l}}^{-3}\tilde{\mathbf{g}}^{\mathrm{T}}\mathbf{M}. \tag{44}$$

If we exploit the fact that $\tilde{\mathbf{z}}$, $\tilde{\mathbf{y}}$, $\tilde{\mathbf{a}}$, $\tilde{\mathbf{l}}$ are diagonal and $\tilde{\mathbf{g}}^{\mathrm{T}}$ is block diagonal, we may write (44) as

$$\frac{\partial \boldsymbol{\lambda}}{\partial \mathbf{p}} = \tilde{\mathbf{y}}\tilde{\mathbf{a}}\tilde{\mathbf{l}}^{-3}\tilde{\mathbf{g}}^{\mathrm{T}}\hat{\mathbf{z}}\mathbf{M}.$$

From (10) we have that,

$$\hat{\mathbf{z}}\mathbf{M} = -\mathbf{C}^{\mathrm{T}}.$$

Finally, the stiffness matrix is written as,

$$\mathscr{K} = \mathbf{C}\tilde{\mathbf{g}}\tilde{\mathbf{y}}\tilde{\mathbf{a}}\tilde{\mathbf{l}}^{-3}\tilde{\mathbf{g}}^{\mathrm{T}}\mathbf{C}^{\mathrm{T}} - \mathbf{C}\hat{\boldsymbol{\lambda}}\mathbf{M}. \tag{45}$$

This stiffness matrix matches its FEM definition for prestressed trusses given in the literature, see, e.g., Murakami and Nishimura (2001). Here, the stiffness matrix is given in a compact form that clearly displays its structure and sparsity pattern. This compact form greatly simplifies the rank analysis.

6. Examples of a symmetric form-finding problem

6.1. The unstable unit plate

The tensegrity plate of Fig. 9 is characterized by a periodic connectivity pattern that exists within the interior of the structure. Its repetitive connectivity unit is shown in Fig. 8. This unit does not represent a smaller equilibrium tensegrity structure regardless of its geometry, in contrast to the unit of the periodic

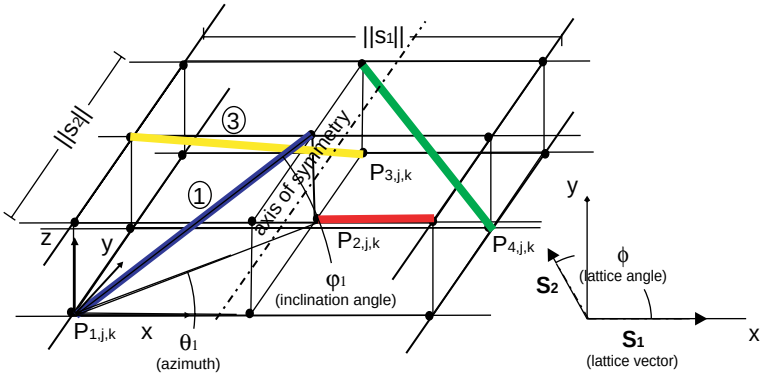

Fig. 8. Connectivity of the unit of the unstable unit plate.

modular tensegrity plates defined in Masic and Skelton (in press). Since the equilibrium of each of the units is provided by interacting with its adjacent units, additional elements must be added to boundary units to allow equilibrium of the whole structure. Its name, *unstable unit plate*, is adopted to reflect these facts.

If the nodes of the plate admit the same periodic pattern, in addition to the periodicity of the connectivity, the resulting plate is not generally an equilibrium tensegrity. This is the case with the left structure of Fig. 9. We define this periodic nodal configuration as a desired geometry $\mathbf{p}_{\text{target}}$ and seek its closest equilibrium configuration, $\mathbf{p}$.

Clearly, the desired periodic geometry $\mathbf{p}_{\text{target}}$ of a periodic plate can be defined by specifying parameters of its lattice, and the geometry of the unit in Fig. 8. This can be done in several ways. A general parametrization of the unit geometry allows that the nodes of its four bars have completely independent positions. The only restriction is that they lay in two separate parallel planes. A way of defining the unit geometry is to specify the positions of the nodes, $\mathbf{p}_{i,j,k}$, $i = 1,\ldots,4$, that all lay in the lower plane of the plate. The parametrization of the unit geometry is completed by defining the bar lengths, and the azimuthal and inclination angles, θ_i and φ_i, of its four bars. The positions of the remaining nodes of the periodic plate are defined by shifting the unit along the two-dimensional lattice defined by two independent vectors $\mathbf{s}_1$, and $\mathbf{s}_2$. If a complete parametrization of a periodic plate geometry is the only objective, restrictions should not be imposed on the lattice parameters. The angle ϕ is used to denote the orientation of the lattice generator $\mathbf{s}_2$ with respect to the generator $\mathbf{s}_1$, and $\mathbf{s}_1$ is chosen to be parallel to the x-axis without loss of generality. This parametrization of the plate periodicity incorporates rectangular, rhombic, square and hexagonal lattices independently from the unit geometry.

The geometry of the periodic plate analyzed in this numerical example is restricted to a less general case. It is assumed that the unit itself admits rotational symmetry about the axis passing through its geometric center as shown in Fig. 8. All the bars of the unit are assigned the same length and share a common inclination angle φ_1. The azimuthal angle of the first bar is denoted θ_1. It completely determines the corresponding angles of the remaining bars, since it is assumed that $\theta_3 = -\theta_1$, and the symmetry defines the azimuths of the two remaining bars. We further assume that the lattice generators $\mathbf{s}_1$ and $\mathbf{s}_2$ are mutually orthogonal and parallel to the corresponding coordinate axes. This pattern yields a rectangular lattice with $\phi = \pi/2$. With these additional restrictions, the nodes and elements of the periodic plate also admit rotational symmetry about the y-axis, which passes through the geometric center of the plate as shown in Fig. 9. In order to exploit the symmetry and simplify the form-finding problem, the boundary elements in the structure of Figs. 9 and 10 are added in such a way that the complete element symmetry of the overall structure is preserved.

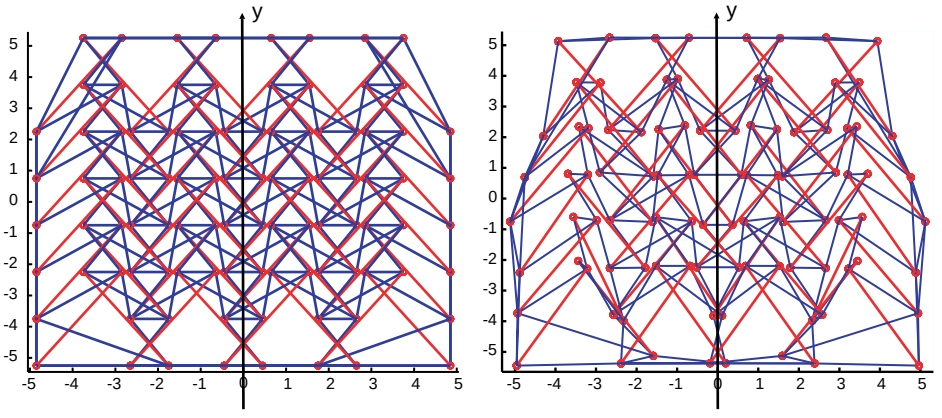

Fig. 9. Top view of the desired plate geometry used also as the initial guess (left), and computed equilibrium plate geometry (right).

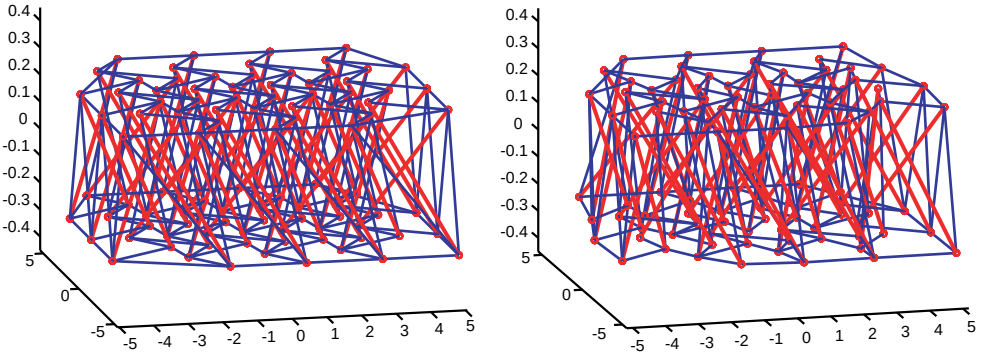

Fig. 10. Isometric view of the initial (desired) plate geometry (left) and computed plate geometry (right).

Recall that this periodic nodal configuration is defined as a desired geometry $\mathbf{p}_{\text{target}}$ with the objective to find its closest equilibrium configuration $\mathbf{p}$. In addition to this soft shape constraint, it is required that the tensegrity equilibrium configuration $\mathbf{p}$ strictly satisfies the plate constraints, and has the same bar lengths l_b and height h_{target} as the desired plate. It is also required that the final plate admit the nodal and element symmetry of the desired plate, and that all the bars of the structure have force-densities larger than $\epsilon > 0$.

First, the connectivity scheme defined by $\mathbb{E}_s$ and $\mathbb{E}_b$ is adopted. The unit vector $\mathbf{n} \in \mathbb{R}^3$ perpendicular to the plate must be provided in order to define the plate. Next, the index i_v of an element e_{i_v} penetrating the plate is identified so that the height of the plate can be constrained to be h_{target}. The matrix $\mathbf{H}$ is constructed to extract the vectors of elements lying in the top and bottom plane of the plate. The desired configuration $\mathbf{p}_{\text{target}}$ is used as the initial guess for the resulting form-finding problem cast as the optimization problem:

$$
\begin{aligned}
&\text{Given data} \quad && \mathbf{p}_{\text{target}}, \mathscr{R}, Q, \mathbf{D}, \mathbf{C}, \mathbf{M}, \mathbb{E}_s, \mathbf{H}, \mathbf{n}, h_{\text{target}}, \mathbf{l}_b, i_v, \epsilon \text{ and } \mathbf{B} \\
&\min_{\underline{\mathbf{p}}, \underline{\boldsymbol{\lambda}}} \quad && F_o(\underline{\mathbf{p}}, \underline{\boldsymbol{\lambda}}) = (\mathbf{p} - \mathbf{p}_{\text{target}})^{\mathrm{T}}(\mathbf{p} - \mathbf{p}_{\text{target}}) \\
& && \text{where } \mathbf{p} = \mathscr{R}\underline{\mathbf{p}}, \quad \boldsymbol{\lambda} = Q\underline{\boldsymbol{\lambda}}, \quad \mathbf{g} = \mathbf{M}\mathbf{p}, \quad \mathbf{g}_b = \mathbf{B}^{\mathrm{T}}\mathbf{p} \\
&\text{such that} \quad && \mathbf{D}\mathbf{C}\hat{\boldsymbol{\lambda}}\mathbf{M}\mathbf{p} = 0, \\
& && \lambda_i \geqslant 0, \quad e_i \in \mathbb{E}_s, \\
& && \lambda_i > \epsilon, \quad e_i \in \mathbb{E}_b, \\
& && (I \otimes \mathbf{n}^{\mathrm{T}})\mathbf{H}\mathbf{g} = 0, \\
& && \mathbf{n}^{\mathrm{T}}\mathbf{g}_{i_v} = h_{\text{target}}, \\
& && \tilde{\mathbf{g}}_b^{\mathrm{T}}\mathbf{g}_b = \tilde{\mathbf{l}}_b\mathbf{l}_b.
\end{aligned}
\tag{46}
$$

The constraint on the length of each element has been expressed as a sum-of-squares rather than a two-norm. This ensures that the constraint derivative is well defined and does not involve the inverse of the element length.

The tensegrity plate form-finding problem (46) is solved numerically using the sparse nonlinear optimization package SNOPT 6.1 developed by Gill et al. (1997). SNOPT is a general-purpose solver that uses a sequential quadratic programming (SQP) method for minimizing a general nonlinear function subject to bounds on the variables and sparse linear and nonlinear constraints (for more details, see Gill et al., 2002). An advantage of using a large-scale optimizer is that the sparse constraint Jacobian is fully exploited during the solution process. The objective and constraint gradients provided to SNOPT are given by:

$$\begin{bmatrix} \dfrac{\partial F_o}{\partial \underline{\mathbf{p}}} \\ \dfrac{\partial F_o}{\partial \underline{\boldsymbol{\lambda}}} \end{bmatrix} = \begin{bmatrix} 2\mathscr{R}^{\mathrm{T}}(\mathscr{R}\underline{\mathbf{p}} - \mathbf{p}_{\mathrm{target}}) \\ 0 \end{bmatrix}, \quad \begin{bmatrix} \dfrac{\partial F_c}{\underline{\mathbf{p}}} & \dfrac{\partial F_c}{\partial \underline{\boldsymbol{\lambda}}} \end{bmatrix} = \begin{bmatrix} \mathbf{DC}\hat{\boldsymbol{\lambda}}\mathbf{M}\mathscr{R} & \mathbf{DC}\tilde{\mathbf{g}}Q \\ 0 & X_s \\ 0 & X_b \\ (I \otimes \mathbf{n}^{\mathrm{T}})\mathbf{HM}\mathscr{R} & 0 \\ \mathbf{n}^{\mathrm{T}}\mathbf{M}_{i_v}^{\mathrm{T}}\mathscr{R} & 0 \\ 2\tilde{\mathbf{g}}_b^{\mathrm{T}}\mathbf{B}^{\mathrm{T}}\mathscr{R} & 0 \end{bmatrix},$$

where $\mathbf{M}_{i_v} = \mathbf{M}(e_{i_v})$ are the rows of $\mathbf{M}$ that correspond to the element e_{i_v}, and X_s and X_b are the matrices that extract corresponding string and bar entries from the full force-density vector.

The number of elements and nodes of the structure are 270 and 96 respectively, yielding an optimization problem that has 282 variables and 360 constraints. The solution of this problem required a total of 27 iterations of the SQP algorithm used by SNOPT. The convergence of the objective function is shown in Fig. 11, and it shows the values of the objective function for both major and minor iterations of the SQP algorithm. Note that the objective value does not converge monotonically. This is because SQP methods satisfy the nonlinear constraints only in the limit and hence the early iterates are not feasible. An estimate of the efficiency of the SQP algorithm on this problem may be determined by the fact that it was necessary to evaluate the problem functions (46) only 39 times in order to locate the solution.

6.2. Shell-class tensegrity tower

In this example, a six-stage shell-class tensegrity tower with four bars per stage is designed. The desired symmetric shape of the structure enables geometry parametrization so that the change of variables defined in (36) is performed. All stages of the structure are constrained to share common geometric parameters. In other words, the number of variables in the vectors $\mathbf{l}_b$, $\mathbf{r}$, $\mathbf{t}$, $\boldsymbol{\alpha}$, $\boldsymbol{\beta}$, $\boldsymbol{\gamma}$ can be reduced to one. It is assumed that the length of the bars l_b, and the structure radius r are given. Further, it is required that the truncation parameter be $\mathbf{t} = \underline{\mathbf{1}}$, and $\beta = 2\pi/n$, which guarantees equal lengths of the saddle strings defined in Skelton et al. (2001). The height of the structure $h = h(n, \mathbf{l}_b, \mathbf{r}, \mathbf{t}, \boldsymbol{\alpha}, \boldsymbol{\beta}, \boldsymbol{\gamma})$ defined in (36), is constrained to be h_{target}.

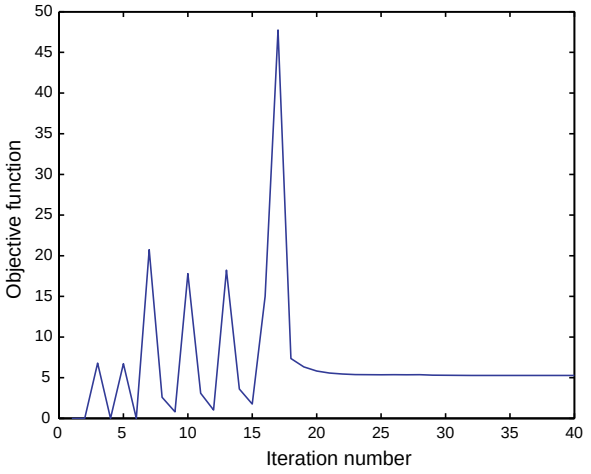

Fig. 11. Convergence of the objective function.

Symmetry of the structure can be exploited to reduce both the number of equations to be solved and the number of force-density variables. The solution of the form-finding problem is obtained by casting the nonlinear constrained zero-finding problem as the optimization problem:

$$\begin{aligned}
&\text{Given data} && \mathbf{C}, \mathbf{M}, \mathbb{E}_s, Q, \mathbf{D}, \mathscr{R}, h_{\text{target}}, n, l_b, r, \mathbf{t}, \beta : \\
&\min_{\alpha,\gamma,\underline{\boldsymbol{\lambda}}} && F_o = (\mathbf{DC}\tilde{\mathbf{g}}Q\underline{\boldsymbol{\lambda}})^{\mathrm{T}}(\mathbf{DC}\tilde{\mathbf{g}}Q\underline{\boldsymbol{\lambda}}) \\
& && \mathbf{g} = \mathbf{M}\mathbf{p}, \quad \mathbf{p} = \mathscr{R}\underline{\mathbf{p}}(n, l_b, r, \mathbf{t}, \alpha, \beta, \gamma) \\
&\text{subject to} && \underline{\lambda}_i \geqslant 0, \quad e_i \in \mathbb{E}_s, \\
& && \|\underline{\boldsymbol{\lambda}}\| > 0, \\
& && h(n, l_b, r, \mathbf{t}, \alpha, \beta, \gamma) = h_{\text{target}}.
\end{aligned}$$

This problem is also solved numerically using the SNOPT package. The objective and constraint gradients are computed analytically and provided to SNOPT. The general form of the objective gradient with respect to the geometric variables $\mathbf{l}_b$, $\mathbf{r}$, $\mathbf{t}$, $\boldsymbol{\alpha}$, $\boldsymbol{\beta}$, $\boldsymbol{\gamma}$, and the force-density variable $\underline{\boldsymbol{\lambda}}$ is:

$$\text{grad} = 2\left[\mathbf{DC}\widehat{Q\underline{\boldsymbol{\lambda}}}\mathbf{M}\mathscr{R}\left[\frac{\partial\underline{\mathbf{p}}}{\partial\mathbf{l}_b} \;\; \frac{\partial\underline{\mathbf{p}}}{\partial\mathbf{r}} \;\; \frac{\partial\underline{\mathbf{p}}}{\partial\mathbf{t}} \;\; \frac{\partial\underline{\mathbf{p}}}{\partial\boldsymbol{\alpha}} \;\; \frac{\partial\underline{\mathbf{p}}}{\partial\boldsymbol{\beta}} \;\; \frac{\partial\underline{\mathbf{p}}}{\partial\boldsymbol{\gamma}}\right] \;\middle|\; \mathbf{DC}\tilde{\mathbf{g}}Q\right]^{\mathrm{T}}(\mathbf{DC}\tilde{\mathbf{g}}Q\underline{\boldsymbol{\lambda}}).$$

Here, we give only the sparsity pattern of the Jacobian of the nonlinear part of the nodal parametrization (36), see Fig. 12.

The resulting optimization problem was solved easily. A total of 110 evaluations of the problem function was required before the algorithm converged, from the initial configuration shown in Fig. 13, to the leftmost structure of Fig. 14.

In addition, the problem was solved for two different values of the height h_{target}. All other data and initial conditions were unaltered. The resulting problems required a total of 100 and 87 iterations before the algorithm converged to the structures depicted in Fig. 14. This incremental procedure using increasing heights illustrates that the technique may be used as the basis of an iterative method for generating feasible paths of tower reconfigurations defined by controlling the string lengths. Such a procedure would use the solution of the previous structure as the start point for the next, leading to further reductions in computing time.

Finally, an example of a shell-class tower structure with tapered stages is given. This example illustrates the generality of the formulation introduced here. The only change from the previous problems is that the desired distribution of the truncation ratio $\mathbf{t}$ is now:

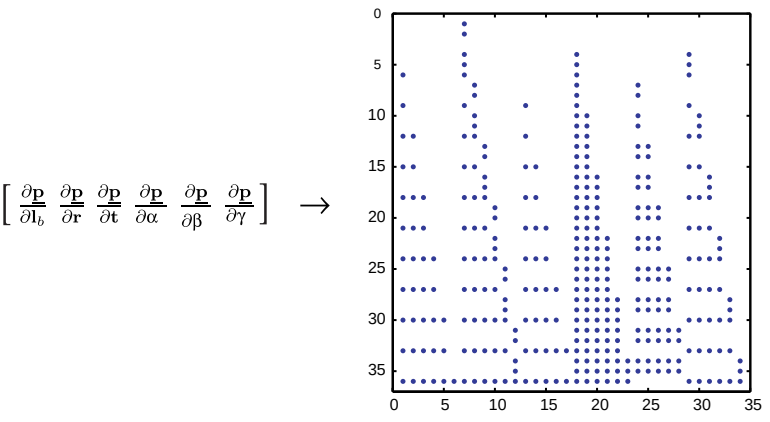

Fig. 12. Sparsity patter of the Jacobian of the mapping between geometric parameters and nodal vector $\underline{\mathbf{p}}$.

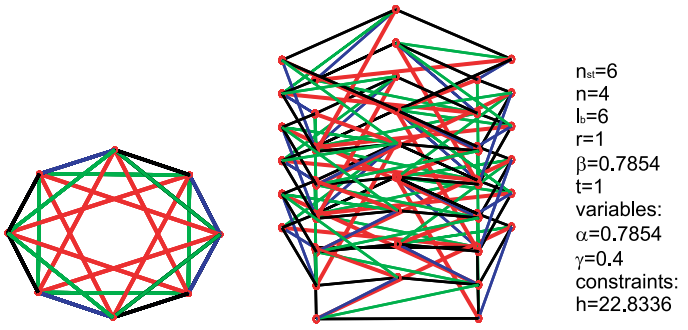

Fig. 13. Top and side view of the initial non-equilibrium configuration of the shell-class tensegrity tower.

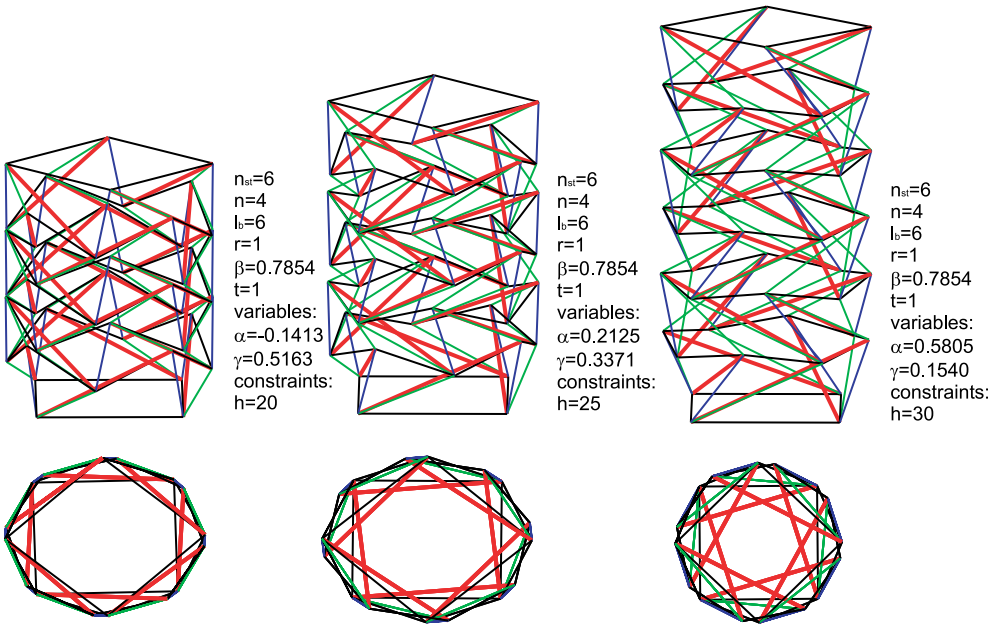

Fig. 14. Equilibrium shell-class tensegrity towers with different heights and common radius.

$$\mathbf{t} = [0.7 \quad 1 \quad 1 \quad 1 \quad 0.8 \quad 1.3]^{\mathrm{T}},$$

while all other constraints and initial conditions remain unaltered. The final structure computed by SNOPT after 177 iterations is shown in Fig. 15.

The reason that the solution of the plate problem requires less iterations than the tower examples is that the constraints are less nonlinear in the first case. The plate problem consists of a quadratic objective function that is subject to the set of linear constraints, bilinear constraints, and quadratic constraints. In contrast to this fairly low level of nonlinearity, the constraints are much more nonlinear in the tower case which can be realized by inspecting the geometric parametrization in (36). The last example of the tower with tapered stages is the most complex problem, see Fig. 16, because of the increased number of variables and level of nonlinearity.

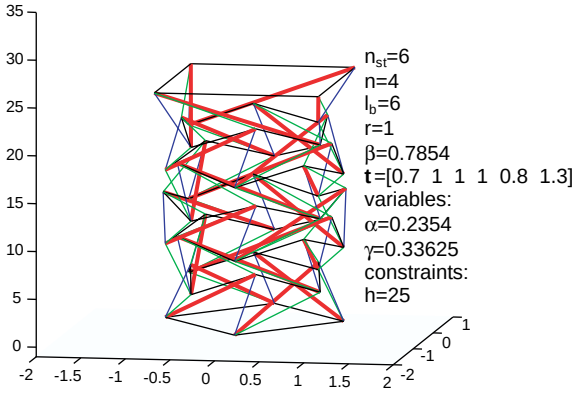

Fig. 15. Shell-class tensegrity with tapered stages.

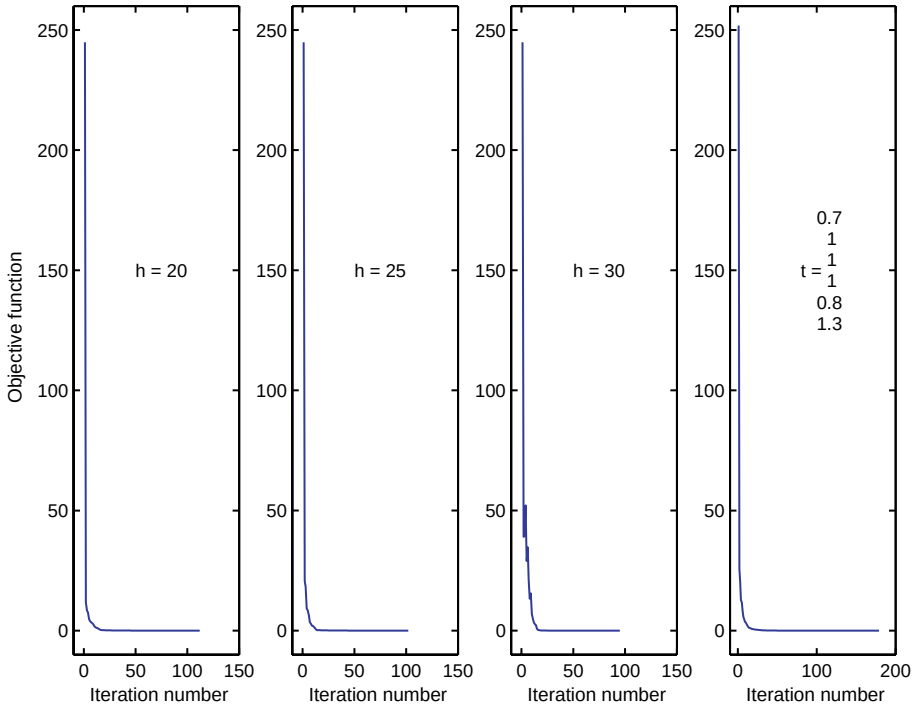

Fig. 16. Convergence of the optimization algorithm for the given examples of cylindrical and tapered towers.

6.3. Discussion

The force-density method for tensegrity form-finding allows for a comprehensive formulation and treatment of shape constraints at no additional expense. Moreover, it appears to be the best method for large-scale problems. First, unlike most other methods it does not require unknown *a priori* knowledge about the structure being designed. For example, the nonlinear programming method of Tibert and Pellegrino (2003) requires advanced knowledge of which elements attain their extreme lengths in equilibrium. Masic (2004)

shows that there exist simple structures that have no elements with extremized lengths in equilibrium, and therefore cannot be handled with this method. In addition, he proposes a modification of the method that corrects the deficiency.

Second, numerical issues related to the solution of non-convex bilinear equilibrium equations are equivalent to those of the energy method, and the non-linear programming method considered by Tibert and Pellegrino (2003), and the modified version of the latter. The reader is referred to Masic (2004), where it is demonstrated that the force-density formulation of the equilibrium equations actually represents the primal-dual form of the necessary optimality conditions for these optimization methods, and that the free force-density variables serve as dual variables.

7. Conclusions

This paper extends the scope of the force-density form-finding method for tensegrity structures by explicitly incorporating shape constraints into the problem. One of the principal contributions of this paper is the use of tensegrity symmetry analysis in the context of the force-density method for form-finding. We study different symmetries of tensegrity structures and propose a systematic and rigorous approach to using symmetry to simplify the problem. The analysis provides the theoretical basis for methods for large-scale problem that use modern numerical optimization tools. These methods allow the rapid solution of tensegrity tower forms that previously could be solved efficiently only in some special cases. The form-finding problem for large-scale tensegrity plates is defined and efficiently solved. The proposed tensegrity invariance transformation defined in the paper enables the solution of the form-finding problem for a large class of tensegrities. It also represents a new tool that can be implemented for the design and control of tensegrity structures.

References

Back, A., Connelly, R., 1998. Catalogue of symmetric tensegrities. Available from: <http://mathlab.cit.cornell.edu/visualization/tenseg/tenseg.html>.

Connelly, R., Back, A., 1998. Mathematics and tensegrity. American Scientist 86 (2), 142–151.

Connelly, R., Terrell, M., 1995. Globally rigid symmetric tensegrities. Structural Topology 21, 59–78.

Gill, P.E., Murray, W., Saunders, M.A., (1997). User's guide for SNOPT 5.3: a Fortran package for large-scale nonlinear programming. Numerical Analysis Report 97-5. Department of Mathematics, University of California, San Diego. La Jolla, CA.

Gill, P.E., Murray, W., Saunders, M.A., 2002. SNOPT: An SQP algorithm for large-scale constrained optimization. SIAM Journal on Optimization 12 (4), 979–1006.

Grunbaum, B., Shepard, G.C., 1986. Tilings and Patters. W.H. Freeman and Company, New York.

Hinrichs, L.A., 1984. Prismic tensigrids. Structural Topology 9, 3–14.

Masic, M., 2004. Design, optimization, and control of tensegrity structures. PhD thesis, University of California San Diego, Department of MAE, La Jolla, CA, USA.

Masic, M., Skelton, R.E., 2004. Optimization of class-2 tensegrity towers. In: Proceedings of the 11th Smart Structures and Materials Conference, vol. 5390. International Society for Optical Engineering (SPIE), Belligham, WA, USA. pp. 163–174.

Masic, M., Skelton, R.E., in press. Path planning and open-loop shape control of modular tensegrity structures. AIAA Journal of Guidance, Control, and Dynamics.

Motro, R., 1984. Forms and forces in tensegrity systems. In: Nooshil, H. (Ed.), Proceeding of Third International Conference on Space Structures. Elsevier, Amsterdam, pp. 180–185.

Murakami, H., Nishimura, Y., 2001. Static and dynamic characterization of regular truncated icosahedral and dodecahedral tensegrity modules. International Journal of Solids and Structures 38 (50–51), 9359–9381.

Schek, H.J., 1974. The force density method for form finding and computation of general networks. Computer Methods in Applied Mechanics and Engineering 3 (1), 115–134.

Skelton, R.E., Pinaud, J.P., Mingori, D.L., 2001. Dynamics of the shell-class of tensegrity structures. Journal of the Franklin Institute 2–3 (338), 255–320.

Tibert, A.G., Pellegrino, S., 2003. Review of form-finding methods for tensegrity structures. International Journal of Space Structures.
Vasart, N., Motro, R., 1999. Multiparametered formfinding method: application to tensegrity systems. International Journal of Space Structures 14 (2), 147–154.